Determining the ultraviolet radiation dose experienced by aerosols using ultraviolet-sensitive dyes

Qingqing Fu, Frank Einar Kruis

Institute of Technology for Nanostructures (NST) and Center for Nanointegration Duisburg-Essen (CENIDE);
Faculty of Engineering, University of Duisburg-Essen, Duisburg, Germany

Correspondence to: Frank Einar Kruis (einar.kruis@uni-due.de)

Keywords: viral aerosols, air disinfection, UVC radiation dose, ultraviolet-sensitive dyes, irradiation chamber

Abstract. The application of ultraviolet (UV) light-based air disinfection methods holds promise, but also presents several challenges. Among these, the quantitative determination of the required UV radiation dose for aerosols is particularly significant. This study explores the possibility of determining the UV dose experienced by aerosols without the use of virus-containing aerosols, circumventing associated laboratory safety issues. To achieve this, we developed a model system comprised of UV-sensitive dyes dissolved in di-ethyl-hexyl-sebacate (DEHS), which facilitates the generation of non-evaporating and UV-degradable aerosols. For the selection of UV-sensitive dyes, 20 dyes were tested, and two of them were selected as most suitable according to several selection criteria. Dye-laden aerosol droplets were generated using a commercial aerosol generator and subsequently exposed to UVC radiation in a laboratory-built UV irradiation chamber. We designed a low-pressure impactor to collect the aerosols pre- and post-UV exposure. Dye degradation, as a result of UV light exposure, was then analyzed by assessing the concentration changes in the collected dye solutions using a UV-visible spectrophotometer. Our findings revealed that a UV dose of 245 mW·s·cm^{-2} resulted in a 10% degradation, while a lower dose of 21.6 mW·s·cm^{-2} produced a 5% degradation. In conclusion, our study demonstrates the feasibility of using aerosol droplets containing UV-sensitive dyes to determine the UV radiation dose experienced by an aerosol.
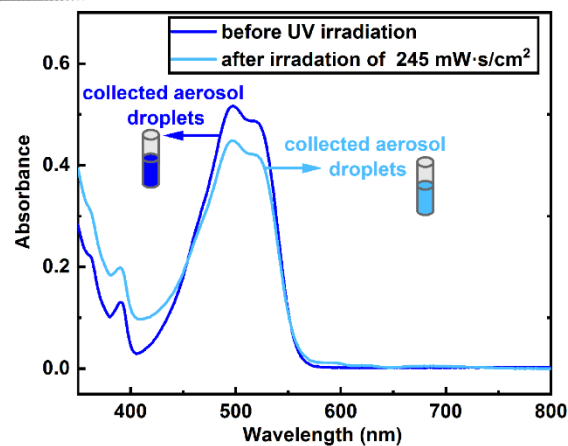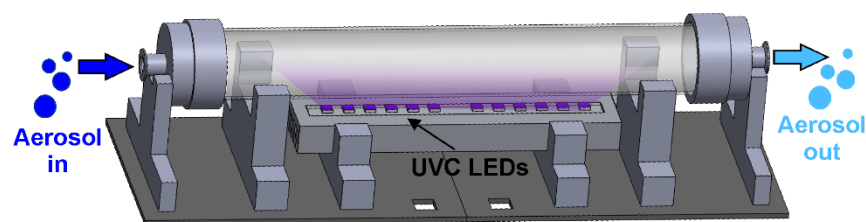
1 Introduction

25 The COVID-19 pandemic, caused by the severe acute respiratory syndrome coronavirus 2 (SARS-CoV-2), has profoundly impacted both individual lives and the global economy (Dong et al., 2020; Priya et al., 2021). The predominant contributor to these effects is the rapid airborne transmission of the virus, often involving aerosols smaller than five µm and traveling distances exceeding one to two meters from the infected individual (Zayas et al., 2012; Wang et al., 2021; Lefebvre et al., 2022). A diverse, integrated approach has been implemented globally

30 in response to this pandemic. Public health measures such as the enforcement of personal protective equipment (PPE) usage, including masks, adherence to social distancing guidelines, and promotion of hand hygiene practices, have contributed to reducing viral transmission to some extent (Muñoz et al., 2021; Leung and Sun, 2020). Vaccination serves as an essential strategy to control the COVID-19 pandemic because an effective vaccine could induce an appropriate immune response. The rapid and groundbreaking advancement in COVID-19 vaccine

35 development by researchers has played a pivotal role in significantly reducing the global impact of the pandemic (2023 Chakraborty et al.). However, developing an effective vaccine is a time-consuming process due to pre-clinical protocols and three-phase clinical trials necessary to ascertain safety and efficacy. Moreover, environmental variations and differences in population densities across geographical areas can cause the viral genome to mutate, which could reduce the efficacy of the developed vaccines (Kaur and Gupta, 2020; Van Dorp

40 et al., 2020)allowing the virus to evade the immune system even after vaccination. Ultraviolet (UV) germicidal irradiation, specifically UVC irradiation within the wavelength range of 200-280 nm (UVC), is known as an effective method for inactivating all known microorganisms and viruses (Abkar et al., 2022; Inagaki et al., 2020; Reed, 2010; Biasin et al., 2021). The UVC radiation is capable of breaking chemical bonds absorption results in the formation of dimeric lesions in the genome of pathogenic microorganisms, which inhibit DNA/RNA

45 replication and inactivate the pathogen (Budowsky et al., 1981; Kowalski, 2009; Beck et al., 2016) (Mankar et al., 2022; Kim and Kang, 2018). Furthermore, UV radiation presents a more environmentally friendly and energy-efficient alternative to liquid disinfectants and heat disinfection for sterilizing liquids, air, and surfaces (Heßling et al., 2020). Therefore, a deeper understanding of using UVC to inactivate pathogenic microorganisms might strengthen our ability to address the public health challenge posed by airborne viruses.

50 A significant challenge lies in the quantitative determination of the UV radiation dose required to inactivate pathogenic microorganisms (Gandhi et al., 2012; Feng et al., 2010). Although researchers have investigated the necessary dose of UV radiation to disinfect coronaviruses, it's noteworthy that the calculated and measured UV dosages in these studies exhibit considerable variations (Walker and Ko, 2007; Buonanno et al., 2020; Tseng and Li, 2005; Terpstra et al., 2007; Pratelli, 2008; Deshmukh and Pomeroy, 1969; Eickmann et al., 2020; Kariwa et

55 al., 2006; Kaur and Gupta, 2020). For instance, even within the 254 nm results, the UV radiation doses required to inactivate 90% of the virus concentration (the log-reduction doses) ranges widely it is 0.6 mW·s·cm⁻² for bovine coronavirus while for SARS (CoV Urbani), it's as high as 11,754 mW·s·cm⁻² (Heßling et al., 2020). For the removal of bovine coronavirus using a UV24 unit (with an airflow of 85 m³/h and a produced UV dose of 19.8 mW·s·cm⁻²), the required dose is 0.6 mW·s·cm⁻² in a room of 244 m³ volume without outside air (Kowalski, 2017).

60 In the case of SARS-CoV (Urbani strain), it's as high as 11,754 mW·s·cm⁻² by applying a UVC light source of 4.0 mW·cm⁻² at a distance of 3 cm to the sample (Darnell and Taylor, 2006). The reasons behind this diversity in reported UV doses remain unclear, but possible factors include differences in culture mediums, experimental

facilities (power of the radiation device, distance between light source and virus sample), or sample conditions (solid surface, liquid, aerosol) (Biasin et al., 2021). So far, the inactivation of viral aerosols by UVC radiation has not been as extensively studied as it has been for liquids and on solid surfaces (Feng et al., 2010; Welch et al., 2018; Hamzavi et al., 2020; Hijnen et al., 2006; Bohrerova et al., 2005). This is partly due to the high vapor pressure of pure water, which leads to an extremely short evaporation time and consequently unstable aerosol droplets. For example, a pure water droplet of 100 nm evaporates in approximately two microseconds (Ferron and Soderholm, 1990). This dynamic change in droplet size can also impact the concentration and susceptibility of airborne microorganisms, presenting a significant challenge to many medical and biological laboratories studying bioaerosols. Moreover, aerosol experts, despite their proficiency in aerosol generation and measurement, often encounter difficulties in conducting direct experiments involving pathogenic microorganisms due to the stringent requirement of biosafety laboratory microorganisms (Burnett et al., 2009; Ahmad et al., 2019). In this regard, bridging the gap between aerosol scientists and biologists is crucial for a faster and more comprehensive understanding of bioaerosol inactivation using UVC radiation.

Tracer methods have been widely used in various scientific and medical disciplines to study biochemical and biophysical processes. The tracer is chosen so that it behaves like the substance being studied but can be easily detected. For instance, fluorescence tracing has become powerful tools in biology and biochemistry for imaging cells and tissues, and tracking the movement of molecules within organisms (Kyrychenko, 2015). Radioactive tracing is particularly useful in medicine, where radioactive tracers (Talaat et al., 2019) are used to image body tissues and organs, highlighting areas of high metabolic activity. Recently, Talaat et al. (Talaat et al., 2019) developed a model to numerically assess the radiation dosimetry of inhaled radioactive aerosols, by coupling computational fluid-particle dynamics (CFPD) and the Monta Carlo (MC) methods. In various studies Furthermore, chemical tracers, such as UV-sensitive dyes, have been tested as model systems to mimic the behavior of pathogenic microorganisms under UV radiation exposure. For example, the degradation of chromophores and fluorophores has been used to measure the radiation doses of UV light with a wavelength of 254 nm, serving as chemical indicators for UV sterilization processes. The decrease in absorbance or fluorescence has been correlated to the radiation dose in $W \cdot s \cdot cm^{-2}$ and the reduction in the concentration of microorganisms such as Escherichia coli, Staphylococcus aureus, and Candida albicans (Putt et al., 2012). Moreover, UV-sensitive dyes have been utilized to develop colorimetric UV dosimeters that monitor sunlight exposure to prevent skin damage. Wang (Wang et al., 2018) demonstrated a wearable wristband that combined with a colorimetric UV film to indicate the UV dose through the discoloration of a purple photodegradable dye under exposure to UV light. The UV sensing film completely discolors to transparency in two hours under a solar simulator, suggesting its potential as an indicator to help individuals avoid skin damage. Various wearable devices containing UV-sensitive dyes were developed to monitor UV exposure, showing that the degree of sun exposure can be quantified with an accuracy rate of 95% by establishing a correlation between the color changes and the dosage of UVA (400-320 nm) and UVB (315-280 nm) radiation received (Kurz et al., 2020). Nevertheless, all these studies involving UV-sensitive dyes focus on assessing the required UV radiation doses either in liquid solutions or on solid surfaces. When UV-sensitive dyes are aerosolized and exposed to UVC light, it is unclear whether the photodegradation of UV-sensitive dyes linearly increases with the UV radiation dose. Therefore, the use of UV-sensitive dyes in studying UV effects on aerosol droplets could potentially provide valuable insights into UV disinfection mechanisms and their efficacy.

This study presents the development of a model system that enables the determination of the UV radiation dose experienced by an aerosol, without the need for using microorganisms. This model system can generate stable aerosol droplets composed of UV-sensitive dyes and a carrier liquid, di-ethyl-hexyl-sebacate (DEHS). The UV dose received by these aerosol droplets during irradiation can be evaluated by tracking changes in the color intensity of the UV-sensitive dyes. Three critical criteria were established for the selection of UV-sensitive dyes: no observable sedimentation, high extinction coefficients in the vicinity of 260 nm, and significant solubility in DEHS. Detailed analysis and discussion were conducted regarding the particle size distribution and number concentration of the aerosol droplets generated from these selected UV-sensitive dye solutions A low-pressure impactor was developed to collect the aerosolized droplets, thus enabling the assessment of dye content within the aerosol samples. The concentration of the UV-sensitive dye in the collected liquid was then determined using a UV-Vis spectrometer. The feasibility of using UVC light-emitting-diode (LED) irradiation to degrade the UV-sensitive dye solution was also evaluated in this work. The UV dose experienced by the aerosols was determined by passing through a designed UVC irradiation chamber with various residence time. Determination of the UV dose experienced by the aerosols was achieved by irradiating the flowing aerosols in a specifically designed UVC irradiation chamber.

2 Experimental details

2.1 Selection of UV-sensitive dye solutions

Due to the dynamic nature of the size of water-based aerosols, DEHS was chosen as the carrier liquid to ensure the generation of stable droplets with extended lifetimes., allowing for accurate online measurements. In aerosol science, DEHS is widely used to generate liquid particles with extended lifetimes due to its extremely low saturation vapor pressure. This quality is crucial for studying particle size effects (Ren et al., 2021; Li et al., 2020). Besides, DEHS aerosols, recommended for aerosol filtration testing, allow for more accurate particle size measurement of spherical liquid particles compared to non-spherical solid particles like salt and test dusts, which tend to agglomerate (Gustavsson, 2003). The first step involved selecting a solution containing DEHS and UV-sensitive dyes. 20 types of non-toxic UV-sensitive dyes, including two water-soluble and 18 fluorescent dyes, were tested for suitability. DEHS (CAS-No.: 122-62-3), Erythrosin B (CAS-No.: 568-63-8), and Indigo Carmine (CAS-No.: 865-22-0) were procured from the Merck Group (Sigma-Aldrich Chemie GmbH, Taufkirchen, Germany), while a fluorescent dye kit (Part Number: DFKIT-COMP) was purchased from the Risk Reactor Inc. (California, United States of America). Detailed information about all the tested UV-sensitive dyes is provided in table 1. Initially, solutions containing DEHS and UV-sensitive dyes were prepared at a concentration of 100 µg·mL^{-1} and left undisturbed for 48 hours. For uniform dye distribution in the aerosol, it's essential to use a DEHS solution that reliably maintains a stable dye concentration, a key factor in producing consistent and stable aerosol particles. Eight of these solutions, which demonstrated no noticeable sedimentation, were selected for further evaluation. The UV-Vis absorbance spectra of these eight dye solutions were then determined using an ultraviolet-visible (UV-Vis) spectrophotometer (Cary 500 UV-Vis-NIR Spectrophotometer, Agilent Technologies, USA). Given the varying susceptibility of different UV-sensitive dyes to UVC exposure, dyes with an absorption peak near 260 nm (below 300 nm in this study) were selected for further study. This is because the chemical structure, crucial for the replication of deoxyribonucleic acid (DNA) and ribonucleic acid (RNA), is more sensitive to UV irradiation near

260 nm, where it also exhibits an absorption peak (Abkar et al., 2022). ~~those with UVC susceptibility similar to deoxyribonucleic acid (DNA) or ribonucleic acid (RNA), were identified for further investigation.~~ As noted by Stegemann et al. (Stegemann et al., 2007), substances are typically classified as 'insoluble' when their solubility is below 100 µg/mL in a solvent. Technique like UV-Vis spectroscopy can be used to estimate the solubility of insoluble substances, particularly with those with very low solubility (such as below 100 µg/mL). In the third stage, the relationship between absorbance and concentration of the dye solutions was analyzed to quantitatively assess their solubility in DEHS. The selected dyes were prepared at concentrations of 20 µg·mL^{-1}, 15 µg·mL^{-1}, 10 µg·mL^{-1}, 5 µg·mL^{-1}, and 1 µg·mL^{-1}, after which their UV-Vis absorbance spectra were measured from 260 nm to 800 nm at two nm intervals. The maximum peak absorbance in the visible region was identified for each dye. According to Beer's law, we expect that the maximal absorbance obtained correlates with the solute concentration, ideally forming a linear standard curve. If the measured data do not exhibit a linear regression, the corresponding substance is excluded. All solutions were prepared with highly accurate graduated pipettes and an analytical balance (XS205, Mettler-Toledo AG, Switzerland). To ensure an accurate representation of the average absorbance values, all concentrations were prepared in triplicate.

Table 1: Summarized information on all the tested UV-sensitive dyes.

Sample No.	Dye Info.	Absorption spectra: λ_{max} /nm	Manufacturer
#1	Erythrosine B	544	Sigma-Aldrich
#2	Indigo Carmine	-	Sigma-Aldrich
#3	DFSB-K427	542	Risk Reactor Inc.
#4	DFSB-K400	497	Risk Reactor Inc.
#5	DFSB-K87	-	Risk Reactor Inc.
#6	DFSB-K41-50	475	Risk Reactor Inc.
#7	DFSB-K44-65	416	Risk Reactor Inc.
#8	DFSB-K52	-	Risk Reactor Inc.
#9	DFSB-K160	435	Risk Reactor Inc.
#10	DFSB-K401	571	Risk Reactor Inc.
#11	DFSB-K413	-	Risk Reactor Inc.
#12	DFWB-K1-60	-	Risk Reactor Inc.
#13	DFWB-K7	-	Risk Reactor Inc.
#14	DFSB-K149	552	Risk Reactor Inc.
#15	DFWB-K250	-	Risk Reactor Inc.
#16	TACID9501	-	Risk Reactor Inc.
#17	DFSB-K184	-	Risk Reactor Inc.
#18	DFSB-K40 & DFWB-K40	-	Risk Reactor Inc.
#19	DFSB-K52-55	-	Risk Reactor Inc.
#20	DFWB-K73-51	-	Risk Reactor Inc.

2.2 Experimental setup for investigation of aerosol~~s~~ containing UV-sensitive dyes

2.2.1 Low-pressure impactor for aerosol droplet collection

To evaluate the concentration changes of dye-laden aerosols, a one-stage low-pressure impactor (LPI) was developed for collecting aerosol droplets both before and after UV irradiation treatment. Under the assumption of no evaporation and complete collection of all aerosol particles, the concentration inside the aerosol droplets should remain unchanged. The LPI design was based on the geometry of an electrostatic precipitator developed at the institute of technology for nanostructures (NST, University of Duisburg-Essen, Duisburg, Germany), as illustrated in Fig 1. The inlet gas flow q could be controlled via different critical orifices to adjust the desired residence time in the UV irradiation zone. The outlet of the LPI was connected to a rotary vane pump (Type 301853, ILMVAC GmbH, Ilmenau, Germany), maintaining the measured pressure inside the impactor chamber at less than 0.22 bar.

As shown in Fig. 1, the distance z between the collecting substrate and the aerosol outlet was 5 mm, and the tube length of circular jet tube was approximately 20 mm. The estimated cutoff Stokes diameter d_{50} for the impactor at various inlet gas flows q of 0.78 L/min, 2.26 L/min, and 8.86 L/min is approximately 1.28 μm, 0.75 μm, and 0.38 μm, respectively. For more detailed information on the calculations, please refer to Appendix A. The collection efficiency of the LPI was determined by comparing the aerosol droplets mass concentration, as obtained by a tapered element oscillating microbalance (TEOM; Model 1405, Thermo Fisher Scientific, Waltham, USA), to the collected liquid mass, under defined aerosol flow and collection time. The impact of sampling using the lab-built impactor on the UV-Vis spectra of UV-sensitive dyes (#4 and #7 in Table 1) was also investigated. UV-sensitive dye solutions at various concentrations (20 μg·mL⁻¹, 15 μg·mL⁻¹, 10 μg·mL⁻¹, 5 μg·mL⁻¹ and 1 μg·mL⁻¹) were applied to generate aerosols using a commercial aerosol droplet generator (AGF 2.0, Palas GmbH, Germany). Droplets of each concentration were collected over a two-hour period using the lab-built impactor, equipped with a 1 mm critical orifice (gas flow 8.8 L·min⁻¹). The collected liquids were transferred to a quartz submicron cuvette (Part number: 6610024100, Agilent Technologies, Santa Clara, USA), having a minimum capacity of 80 μL (external dimensions: 45×12.5×12.5 mm, opening aperture: 10 mm, path length: 10 mm), for UV-Vis spectra measurements. The corresponding concentration of dye solutions was determined using the previously mentioned
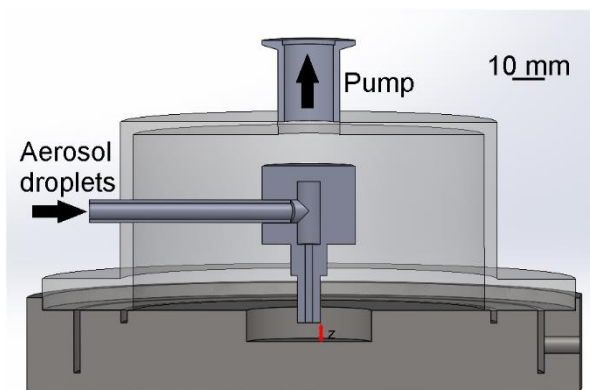
Figure 1: Schematic of the designed low-pressure impactor for aerosol collection in this study.
UV-Vis spectrophotometer.

2.2.2 UV irradiation of UV-sensitive dyes

Before constructing the UV irradiation chamber, a UVC LED module with a peak and dominant wavelength of 275 nm (part number: 37337, Lumitronix LED-Technik GmbH, Hechingen, Germany) was employed to assess whether the selected dyes would degrade upon UV irradiation. As depicted in Fig. 2, one milliliter of the dye solutions was added to the aforementioned cuvette (external dimensions: 45×12.5×12.5 mm, opening aperture: 10 mm, path length: 10 mm) used for measuring collected aerosol droplets. A specially designed 3D-printed fixture, as shown in Fig. 2a, held the quartz cuvette in a fixed position as it underwent irradiation for various durations. A UV light meter (UV-integrator Typ D, Beltron GmbH, Roedermark, Germany, with a spectral measurement range of 250-410 nm) was used to measure the radiation intensity (mW·cm⁻²) at the same position. The detector of this UV light meter has a circular area with a 10 mm diameter, matching the opening aperture of the cuvette used in this work. UV radiation dose (mW·s·cm⁻²) was calculated by multiplying the measured intensity (mW·cm⁻²) by the irradiation duration (seconds). The UV-Vis absorbance spectra of the dye solutions were recorded both before and after irradiation.
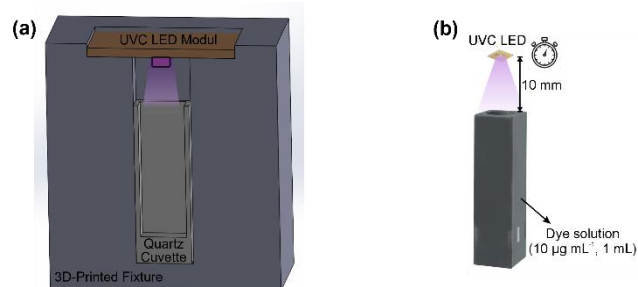
Figure 2: Experimental apparatus, including (a) a view with 3D-printed fixture and (b) a simplified view, used to study the dye solution degradation upon UVC irradiation.

Figure 3a shows a schematic overview of the aerosol irradiation chamber. The constructed chamber comprises a quartz tube, a UVC LED array, and 3D printed fixtures. The quartz tube, with a length of 500 mm, a wall thickness of 2.5 mm, and an internal diameter of 60 mm, was purchased from GVB GmbH - Solutions in Glass (Herzogenrath, Germany). The UVC LED array (Part number: ILS-XN12-S260-0280-SC201-W2, Intelligent LED Solutions, Berkshire, United Kingdom) consists of 12 UVC LEDs (with a radiation peak at 270 nm) that are connected and arrayed linearly to electronic printed circuit boards (PCB). A heat sink and two cooling fans were implemented to enhance the performance of the UV LEDs by dissipating heat from the PCB. ~~In this setup,~~ Figure 3b demonstrates the position of the UVC LED array ~~was positioned with~~ so that its surface is parallel to the bottom of the quartz tube. ~~, at a one centimeter distance~~ The distance, denoted as h, between the LED and the central aerosol flow measures 45 mm. The UV light traveled through the quartz tube and irradiated the flowing aerosols within the chamber. The slanted shaded region in Figure 3b illustrates the calculated effective irradiated volume V ($V = \pi \cdot (D/2)^2 \cdot L$) of the UV chamber. The intensity of the UV radiation is adjustable by modulating the current of the UVC LED array (300-1050 mA). A radiometer, equipped with a ~~UV-3726-5~~ cylindrical **detector** (X1-UV-3726-5 ~~X1-5~~, Gigahertz Optik GmbH, Tuekenfeld, Germany) and calibrated with a 260-290 nm LED, was applied for the measurement of the UVC radiation intensity. The cylindrical detector has a height of 32 mm and a diameter of 37 mm, with its optical detection area being a circle of 11 mm in diameter. To assess the ~~average~~ radiation intensity inside the chamber, a detector fixture was designed to position the detector surface at half the height of the chamber. It should be noted that the intensity measured along the center line might not accurately represent the intensity experienced by all particles. Predicting the equivalent radiation intensity for aerosol droplets in the UV chamber requires developing simulation models, which was not addressed in this study. These mathematical models would need to consider numerous factors, including the optical field of UV irradiation (accounting for reflections and refractions at interfaces between air, quartz, and nitrogen) and the flow field, which affects UV scattering and shadow effects related to particle sizes and trajectories (Kowalski, 2009). Therefore, in our research, we utilized the irradiation intensity measured at the chamber's largest cross-section to inform feedback for our reactor design. The UV intensity experienced by an aerosol droplet was then ~~determined~~ estimated by averaging the measured intensities at five different spots. The exposure time t of the aerosol to the UV radiation is approximated by the mean residence time of the aerosol in the device, defined as $t = V/q$, with V the effective irradiation volume of the quartz tube (777 cm^3) and q the aerosol flow rate. Table 2 summarizes the specifications of the UV chamber and the calculated UV dose used in this study.

Table 2: Specifications of the UV irradiation chamber applied in this study to irradiate aerosols.

UV irradiation chamber with various dose settings			
Critical orifice	0.3 mm	0.5 mm	1.0 mm
Calibrated gas flow q	0.78 L·min^{-1}	2.26 L·min^{-1}	8.86 L·min^{-1}
Chamber irradiation length L	275 mm	275 mm	275 mm
Chamber internal diameter D	60~~0~~ mm	60~~0~~ mm	60~~0~~ mm
Distance between LED and aerosol h	45 mm	45 mm	45 mm
Irradiated volume $V = \pi \cdot (D/2)^2 \cdot L$	777 cm^3	777 cm^3	777 cm^3
Exposure time $t = V/q$	59.8 s	20.6 s	5.3 s
UVC LED current	1000 mA	1000 mA	1000 mA
Calibrated intensity	4.10 mW·cm^{-2}	4.10 mW·cm^{-2}	4.10 mW·cm^{-2}
UV radiation dose	245.1 mW·s·cm^{-2}	84.6 mW·s·cm^{-2}	21.6 mW·s·cm^{-2}
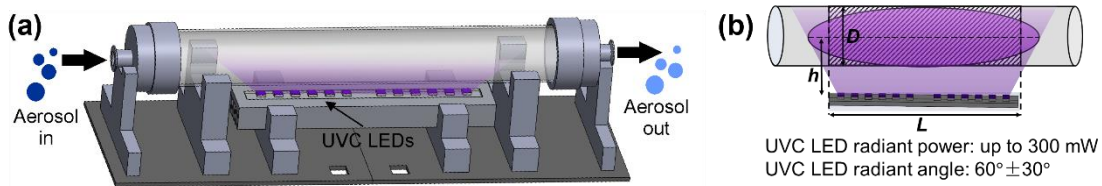
Figure 3: Schematic overview of the constructed UV irradiation chamber (a) and a simplified diagram for the calculation of UV radiation volume and dose (b).
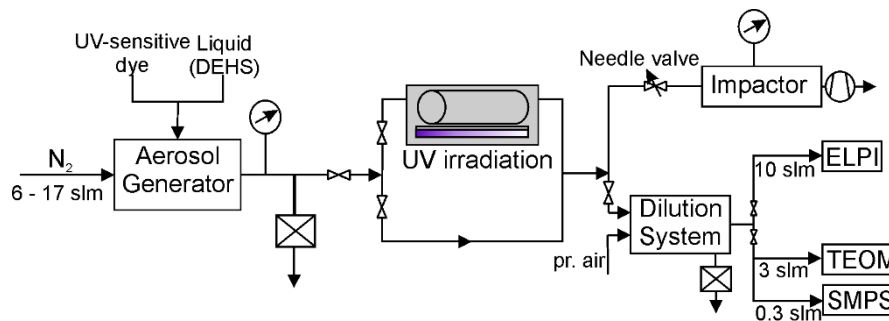
Figure 4: Experimental setup to investigate the effect of UV irradiation on the concentration of aerosol droplets before and after irradiation.

2.2.3 Characterization of aerosol droplets containing UV-sensitive dyes

Figure 4 presents the schematic of the ~~overall~~experimental setup for studying aerosol droplets containing UV-sensitive dyes. ~~Brirely~~Briefly, a liquid nebulizer featuring a two-substance nozzle and a cyclone ($d_{p, max}$ = 2 µm) was used to generate aerosols from the selected UV-sensitive dye solutions. Due to centrifugal force, the cyclone can efficiently separate larger particles generated from the nebulizer. Heavier particles (particles with an aerodynamic diameter > 2 µm) are collected in a liquid reservoir, while the lighter particles are released with the gas flow. The aerosol particle size distribution and concentration, both before and after passing through the designed UV irradiator, were investigated using online measurements. This study applied conventional aerosol measurement devices, including a scanning mobility particle sizer (SMPS; Model 3938, TSI, Minneapolis, USA), an electrical low-pressure impactor (ELPI; Model ELPI+, Dekati Ltd., Tampere, Finland), and a tapered element oscillating microbalance (TEOM). The SMPS device comprises three main components: an aerosol neutralizer (TSI Model 3088), a differential mobility analyzer (DMA, TSI Model 3081) and a condensation particle counter (CPC, TSI Model 3775). In this setup, the DMA employed closed-loop system for the sheath flow, whereas the aerosol flow through the entire SMPS system was regulated by the CPC, which maintained at a low flow rate of

0.3 slm (standard liter per minute). The sheath flow rate for the DMA was set to 3 slm to achieve an aerosol to sheath flow ratio of 1: 10. In the ELPI, particles are classified into 14 size fractions using a cascade impactor. The cutoff aerodynamic sizes are 0.016 µm, 0.03 µm, 0.053 µm, 0.093 µm, 0.15 µm, 0.26 µm, 0.38 µm, 0.60 µm, 0.95 µm, 1.6 µm, 2.5 µm, 3.7 µm, 5.4 µm, and 10.0 µm, respectively. Additionally, to account for the influence of multiply-charged particles on the measured signal, a multiple charge correction was used to the measurements obtained by both ELPI and SMPS. An aerosol dilution system with a dilution ratio of 100 (VKL10 + VKL10 cascade system, Palas GmbH, Karlsruhe, Germany) was utilized to lower the particle number concentration for the standard online instruments. This dilution technique did not significantly alter the particle size distribution (Helsper et al., 1990). The above-mentioned low-pressure impactor was employed to collect aerosols before and after passing through the designed UV irradiation chamber, to characterize how the selected dyes would degrade upon UV irradiation. A UV-Vis spectrophotometer was used to determine the changes in dye concentration of the collected liquids before and after UV irradiation.

3 Results and discussion

3.1 Generation of an aerosol containing UV-sensitive dyes

3.1.1 Selection of UV-sensitive dyes with high solubility in DEHS (three criteria)

Table 3: Comprehensive overview of measurements conducted for UV-sensitive dye selection.

Sample No.	Type of dye	Absorption spectra: λ_{max} /nm	Step 1 Sedimentation	Step 2 UV-Vis absorbance	Step 3 Linear relationship
#1	Water soluble	544	✓	✓	✕
#2	Water soluble	-	✓	✕	✕
#3	Oil soluble	542	✓	✓	✓
#4	Oil soluble	497	✓	✓	✓
#5	Oil soluble	-	✓	✕	✕
#6	Oil soluble	475	✓	✓	✓
#7	Oil soluble	416	✓	✓	✓
#8	Oil soluble	-	✓	✕	✕
#9	Oil soluble	435	✓	✓	✕
#10	Oil soluble	571	✓	✓	✕
#11	Oil soluble	-	✓	✕	✕
#12	Oil soluble	-	✓	✕	✕
#13	Oil soluble	-	✓	✕	✕
#14	Oil soluble	552	✓	✓	✕
#15	Oil soluble	-	✓	✕	✕
#16	Oil soluble	-	✓	✕	✕
#17	Oil soluble	-	✓	✕	✕
#18	Oil soluble	-	✓	✕	✕
#19	Oil soluble	-	✓	✕	✕
#20	Oil soluble	-	✓	✕	✕

As noted earlier, due to the rigorous requirements of biosafety laboratories limit many aerosol laboratories are often unable to conduct experiments from experimenting with pathogenic microorganisms (Burnett et al., 2009; Ahmad et al., 2019). Some researchers, therefore, use smoke aerosols to simulate pathogenic microorganism in their aerosol studies (Chen et al., 2021). In this study, DEHS was chosen as the carrier liquid for generating non-biological and stable aerosol droplets, due to its extremely low saturation vapor pressure (Li et al., 2020). Consequently, a key criterion for selecting suitable UV-sensitive dyes was their high solubility in DEHS. Solubility, the ability of one substance to dissolve in a solvent, can range from infinite to virtually insoluble, and the threshold

value definition varies depending on the application. To rapidly screen UV-sensitive dyes soluble in DEHS, solutions were prepared at a dye concentration of 100 µg·mL-1, aligning with the concentration used by Putt et al. (Putt et al., 2012), who studied chromophore degradation in water solutions for evaluating UV radiation doses.

270 These solutions were then left undisturbed for 48 hours, during which the sedimentation process was recorded, as demonstrated in Fig. 5. From theses visual observations, eight solutions with no significant sedimentation were chosen for the next step: dyes #1, #3, #4, #6, #7, #9, #10, and #14. An overview of all measurements conducted for the selection of UV-sensitive dyes is provided in Table 3

275 The ultraviolet light spectrum theoretically ranges from 100 to 480 nm and is divided into four regions: UVA (320-400 nm), UVB (290-320 nm), UVC (200-290 nm), and VUV (100-200 nm). ~~UVC radiation is the most potent for pathogen inactivation as the maximum absorbance of DNA and RNA occurs around 260 nm.~~ UVC radiation is highly effective for pathogen inactivation, given that DNA and RNA exhibit maximum absorbance around 260 nm when exposed to UVC wavelengths exceeding 240 nm (Heßling et al., 2020; Fujimoto et al., 2023).

280 Consequently, another key criterion for selecting a UV-sensitive dye is its high absorption capacity around 260 nm. For this consideration, the UV-Vis absorbance spectra of all eight dye solutions were measured. It should be mentioned that pure DEHS liquid was used as the baseline, and all spectra were derived by subtraction this baseline. As depicted in figure 6a, while pure water has no absorption upon UV-Vis light, the chosen carrier liquid, Di-ethyl-hexyl separate (DEHS), significantly absorbs UV light with wavelengths below 300 nm. Since the absolute

285 absorbance of DEHS below 270 nm exceeds 1, the UV-visible spectra ranging from 270 to 800 nm were utilized as the baseline for measuring the spectra of pure dyes in this study. Variations in dye concentration were identified through characteristic absorption peaks within the visible spectrum. Figure 6b shows three DEHS baselines obtained by various batches of liquid. As the absorbance fluctuations are smaller than ± 0.001, the error caused by subtracting this baseline should be smaller than 1 %. The similarity of these spectra led to their division into three

290 groups. As detailed in Fig. ~~6~~7, it can be observed that two of the tested dyes (categorized as Group A) might undergo chemical reactions or polarization with DEHS liquid, as indicated by ~~broad absorption peaks~~ their UV-Vis spectra. These spectra show absorption across the whole visible wavelength spectrum and the absorption peaks appear broadened and obscured. For a given organic chromophore, the absorption peaks or shoulders are common for the presence of the conjugated systems and might become broad when extensive conjugation occur with the

295 solvent dependent (Hemdan, 2023; Zheng et al., 2018). Sharp absorption peaks in UV-Vis spectroscopy are desired in this study to quantitatively evaluate concentration changes after UV irradiation.
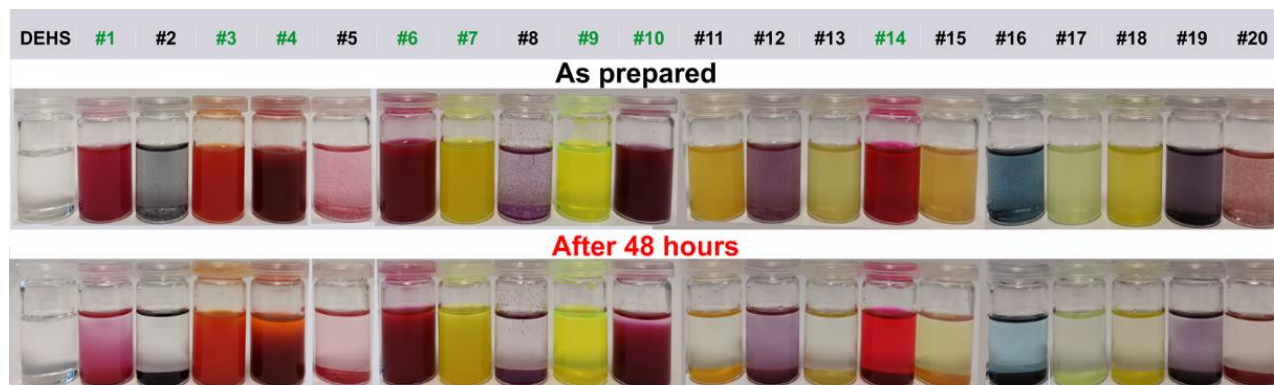
Figure 5: Sedimentation observation of 20 various dye solutions.
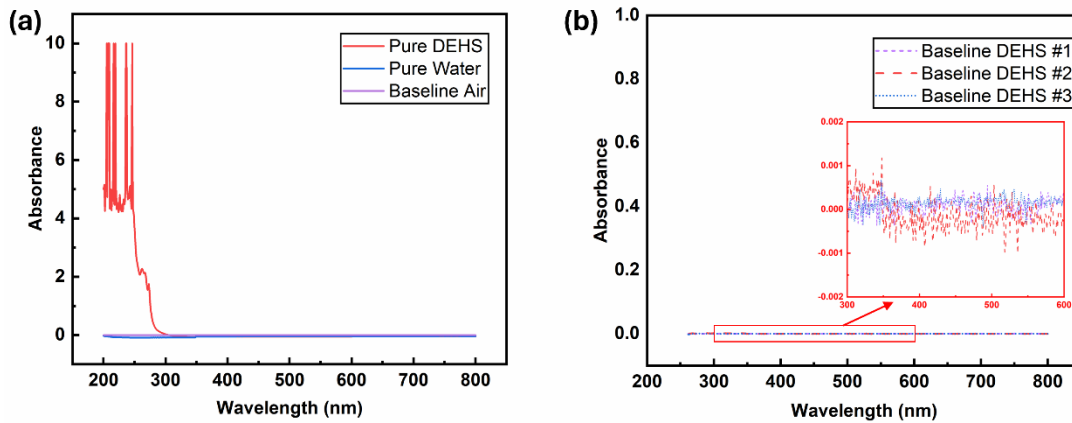
Figure 6: (a) UV-Vis spectra of water and DEHS when using air as the baseline and (b) Baselines obtained from measurements with different batches of DEHS.
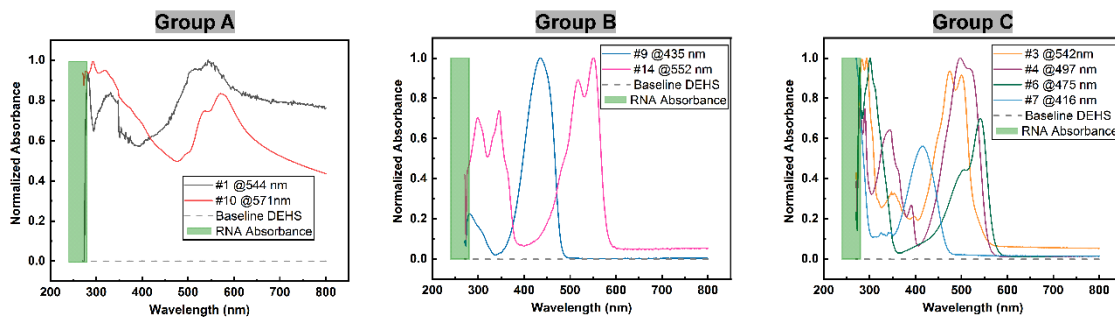
Figure 67: UV-Vis Spectra of dye solutions, where only group C is suitable due to their absorption characteristic in the vicinity of 260 nm and in the visible region.
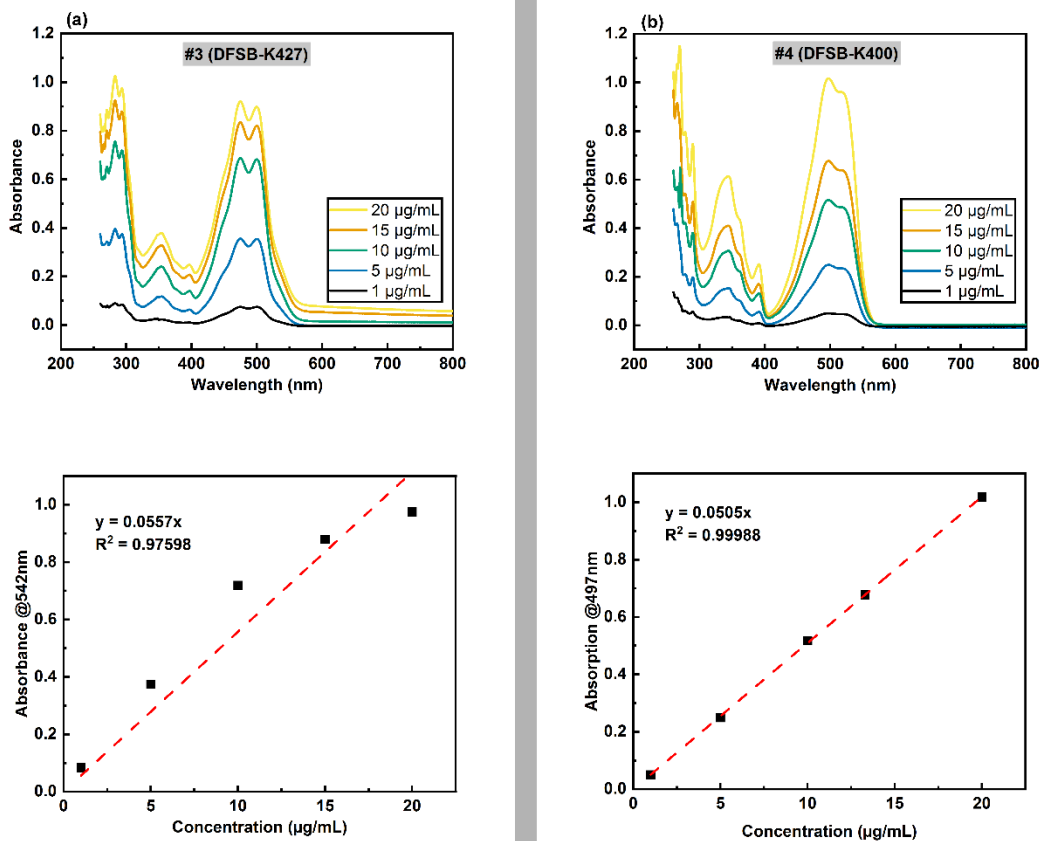
Figure 78: UV-Vis spectra with various concentrations (top) and the corresponding standard curve for dye solutions (bottom), where #3 (left) is the typical example of unsuitable dye and #4 (right) is an example of suitable dye.

Thus, the Group A dyes were deemed unsuitable for further investigation. In contrast, the two dyes categorized as Group B displayed sharp absorption peaks in the visible region. For comparison, all spectra were normalized at the wavelength where maximal absorption peak occurs. Since the maximum absorbance of DNA/RNA is near 260 nm when apply UVC light above 240 nm, dyes with obvious absorbance below 300 nm, which we assume to be around 260 nm, are desired. However, these Group B dyes failed to show significant absorption characteristics near the desired range, leading to their exclusion from subsequent studies. Only four dyes, assigned to Group C, fulfilled this criterion. These dyes displayed distinct absorption characteristics near 260 nm (below 300 nm in this study) and sharp absorption peaks in the visible region.

To ensure a homogeneous dye distribution within the aerosol droplet, it is essential to have a high dissolution rate for the selected dye in the DEHS solvent. The correlation between the absorbance and the concentration of the dye solutions was examined to quantitatively evaluate the solubility level of the chosen dyes (#3, #4, #6, #7 in Tab. 1). Figure 78 presents the typical UV absorption spectra of an unsuitable dye (#3) and a suitable dye (#4) with concentration ranging from 1 µg·mL^{-1} to 20 µg·mL^{-1}. A linear fit was established for each dye based on the maximum absorbance in the visible spectrum region. The results revealed that two of the tested dyes (#4 and #7) had a goodness of fit (R-squared) value greater than 0.99 in a simple linear regression, suggesting superior dissolution and long-term stability in DEHS. As a result, these two dyes (#4 and #7) with higher linearity were selected as candidates for the model system in this research study, as dye degradation was used to quantifyestimate the UV radiation dose.

3.1.2 Effect of the addition of UV-sensitive dyes on the particle size distribution

Our main objective was to develop a stable dye-laden aerosol model to estimate the UV radiation dose experienced by an aerosol droplet. Previous research has suggested that most exhaled aerosol droplets are smaller than 5 µm, including aerosols produced by breathing, speaking, and coughing(Wang et al., 2021; Fabian et al., 2011). More recent studies have shown that aerosols smaller than 1 µm pose significant concern regarding disease transmission since these smaller particles remain in the air longer and can deposit in the respiratory tract to initiate infection (Wang et al., 2018). Therefore, this study on determining the UVC radiation dose required for aerosols primarily focused on evaluating smaller particle-sized aerosols ($d_{CMD} < 1$ µm). A commercial aerosol generator was employed to atomize DEHS liquid, where the carrier gas flow is adjustable by setting the operation pressure of compressed nitrogen. The aerosol generator was equipped with a cyclone ($d_{p, max} = 2$ µm) so that aerosols larger than 2 µm would not leave the generator.

Figure 89 shows the particle size distribution, based on the mobility equivalent diameter measured by SMPS and the Stokes diameter measured by ELPI, of DEHS aerosols produced at various operating pressures of the aerosol generator. The SMPS measurement is based on the electrical mobility of particles, whereas ELPI relies on the aerodynamic properties of the particles. It is evident that an increase in the operating pressure correspondingly increased the particle number concentration., Table 4 presents a summary of the calculated count median diameter (CMD) and the geometric standard deviation (GSD) of the total aerosol population, as measured by ELPI and SMPS. While ELPI measurements show CMD values ranging from 505 nm to 639 nm, with GSD decreasing from 1.76 to 1.35 as pressure increases. SMPS results indicate consistently lower CMD values between 297 nm and 305 nm, with a similar downward trend in GSD from 2.05 to 1.81. This discrepancy could be due to the different measurement principles and sensitivities of these measure instruments. while the particle size distribution

 ~~remained relatively unchanged.~~ Regardless of the operating pressure, ~~T~~the generated aerosol droplets exhibited a size distribution similar to that of most respiratory droplets, with a large fraction is smaller than 1 µm and a peak around 0.2 to 0.8 µm (Morawska et al., 2009; Zayas et al., 2012; Fabian et al., 2011). Furthermore, the particle number concentration of the DEHS droplets produced at a pressure of 2.0 bar aligns closely with the concentration of the cough-generated droplets (Zayas et al., 2012). For these reasons, a pressure of 2.0 bar (generating 9 slm aerosol flow) was chosen to produce DEHS aerosols in subsequent studies.
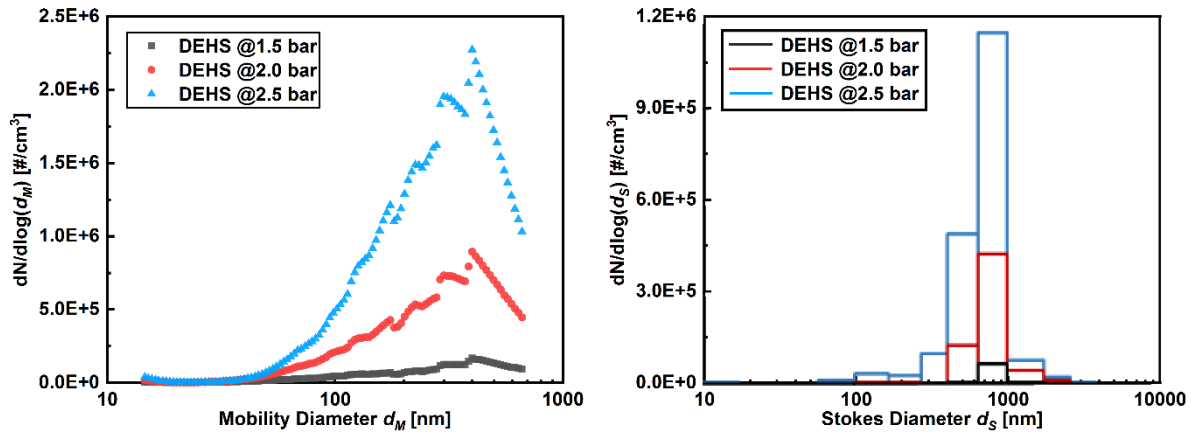
Figure ~~8~~9: Particle size distribution of DEHS aerosols at various operating pressures of the aerosol generator, as measured by SMPS (left) and ELPI (right).

 Table 4 summary of the calculated Count Median Diameter (CMD) and the Geometric Standard Deviation (GSD) of the total aerosol particles, which were determined by ELPI and SMPS.

Aerosol Generator	ELPI		SMPS	
using pure DEHS	CMD	GSD	CMD	GSD
1.5 bar	516 nm	1.76	305 nm	2.05
2.0 bar	505 nm	1.45	301 nm	1.91
2.5 bar	639 nm	1.35	297 nm	1.81
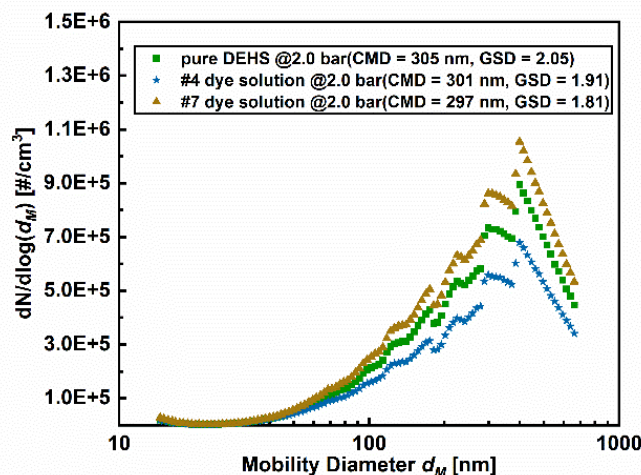
Figure ~~9~~10: Comparison of particle size distribution (measured by SMPS) of aerosols generated from dye solutions and pure DEHS, respectively.

In addition, the influence of adding UV-sensitive dye on the particle size distribution of DEHS aerosols was investigated. The previously selected dyes, either #4 or #7, were dispersed in DEHS liquid to prepare dye solutions with a concentration of 10 µg·mL^{-1}, respectively. These prepared dye solutions were fed into the aerosol generator,

 which was subsequently driven by a pressure of 2.0 bar to generate droplets containing UV-sensitive dyes. Figure

910 displays the particle size distribution and number concentration of the generated dye-laden droplets as well as pure DEHS droplets. For pure DEHS, the measured CMD by SMPS is 305 nm with a GSD of 2.05. When UV-sensitive dye #4 and #7 are introduced in DEHS, the CMD marginally decreases to 301 nm and 297 nm, respectively, along with a reduction in GSD to 1.91 and 1.81. All measurements, including aerosol generation and online characterization, were conducted continuously over a one-hour period. Based on these experimental observations, the slight fluctuation in the number concentration is likely due to ~~the instability of the aerosol generator~~ factors inherent to the commercial aerosol generator, such as the instability of pre-pressure regulation. Therefore, it can be concluded that the addition of UV-sensitive dyes (at 10 µg·mL^{-1}) does not significantly affect the particle size and number concentration of DEHS aerosols.

3.2 Effect of impactor sampling on dye content in aerosols

Sampling airborne pathogens poses significant challenges as most bioaerosols are water-based, and their particle size can change due to evaporation during the sampling process (Verreault et al., 2008). In this study, DEHS, an oily liquid, was chosen to generate aerosols, eliminating the complexity associated with liquid evaporation. A lab-built impactor, as described in figure 1, was designed to collect dye-containing droplets before and after their passage through a UV irradiation chamber. ~~The aerosol mass concentration was directly measured online using a TEOM to and then estimate the collection efficiency.~~ The mass output of the aerosol generator was determined by directly measuring the aerosol mass concentration online using a commercial TEOM device, and this data was then used to estimate the collection efficiency of the LPI. Concurrently, aerosol droplets were collected using the impactor at a defined aerosol flow rate (8.8 L·min^{-1}) for one hour, ensuring an adequate liquid volume (minimal 80 µL for the submicron quartz cuvette) for UV-Vis measurements. Dye solutions #4 and #7 with concentrations ranging from 1 µg·mL^{-1} to 20 µg·mL^{-1} were utilized for these measurements. The collection efficiency was determined to be above 90% by comparing the mass output of the aerosol generator to the collected liquid. The missing 10% of aerosol mass is likely from smaller droplets not collected by the impactor, given that the estimated cutoff size (Stokes diameter) d_{50} of the impactor at a flow rate of 8.8 L/min is 0.38 µm. Moreover, the absorbance of all collected liquids was measured to compare the concentration with those in the liquid reservoir of the aerosol generator, as demonstrated in Fig. ~~10~~11.
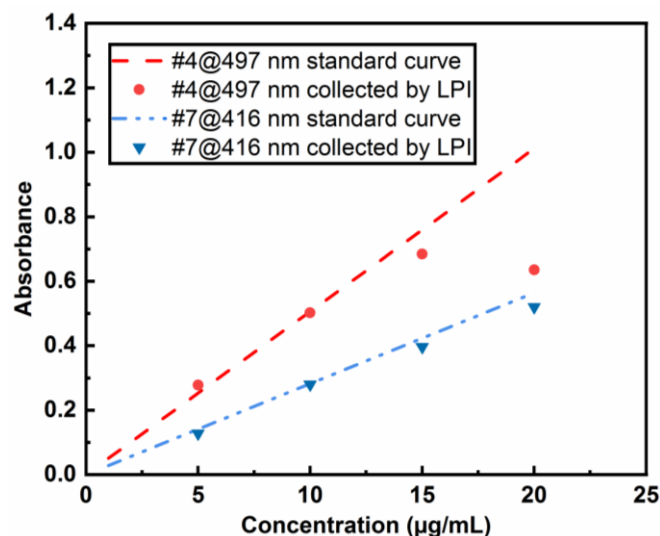
Figure ~~10~~11: Effect of LPI collection on the dye concentrations by using various concentrations of dye solutions.

Notably, concentration deviations became increasingly pronounced when higher concentrations of dye solutions (> 15 µg·mL⁻¹) were used to generate aerosols. ~~This observation could potentially be explained by the various various concentration (maximal concentration for a droplet)within a droplet dependence of the dye concentration in a droplet on the size of the droplet.~~ ==This observation might be attributed to the differing concentrations within individual droplets, a hypothesis that can be further substantiated by collecting categorized droplets with varying diameters.== ~~Both the measured and theoretically calculated results revealed that the maximal collection volume of DEHS droplets, using the aerosol generator AGF 2.0 at a pressure of 1.5 bar, was at 96 µL·h⁻¹.~~ ==Using the AGF 2.0 aerosol generator at 1.5 bar, the mass output m, as measured by the TEOM instrument, is 88 mg·h⁻¹. Consequently, the maximum collection volume V of DEHS droplets, calculated as $V = m / \rho_P$ (with ρ_P=0.912 g·cm⁻³), amounts to 96 µL·h⁻¹.== In the current study, a one-stage impactor was developed to capture the generated polydisperse droplets for UV-Vis spectrum analysis, which expedited the collection process and efficiency. However, this approach did not consider the potential influence of droplet size on the dye concentration and degradation. Future studies should generate or classify narrower aerosol fractions instead of a broad aerosol distribution to investigate potential particle size effects. To mitigate the effect of dye concentration deviation, a concentration of 10 µg·mL⁻¹ was employed, ensuring that each dye (#4, #7) remained well within the linear range for the UVC degradation studies.

3.3 Determination of dye degradation of selected UV-sensitive dyes

~~Currently, most UV disinfection systems for water, air, and surfaces continue to utilize conventional low- or medium-pressure mercury lamps. The primary concern with these lamps is their fragility and their containment of toxic mercury, which poses environmental hazards and requires proper disposal. UV LEDs, on the other hand, are emerging as a popular, environmentally-friendly alternative. Their compact size simplifies their integration into sterilization systems, and they offer a diverse range of wavelengths (Kim and Kang, 2018; Song et al., 2016). Considering the above reasons, this study employed UVC LEDs to investigate dye degradation upon UV radiation.~~ ==In this study, UVC LEDs were utilized to explore the degradation of dyes under UV radiation. Traditional low- or medium-pressure mercury lamps, although effective, raise concerns due to their fragility and the presence of toxic mercury, posing environmental hazards and necessitating proper disposal. Conversely, UV LEDs are emerging as a favored and eco-friendly alternative (Chiappa et al., 2021). Their compact size facilitates easy integration into sterilization systems, and they provide a wide range of wavelengths (Kim and Kang, 2018; Song et al., 2016).== To characterize the degradation of the selected UV-sensitive dyes upon UV irradiation, 1 ml of a 10 µg·mL⁻¹ dye
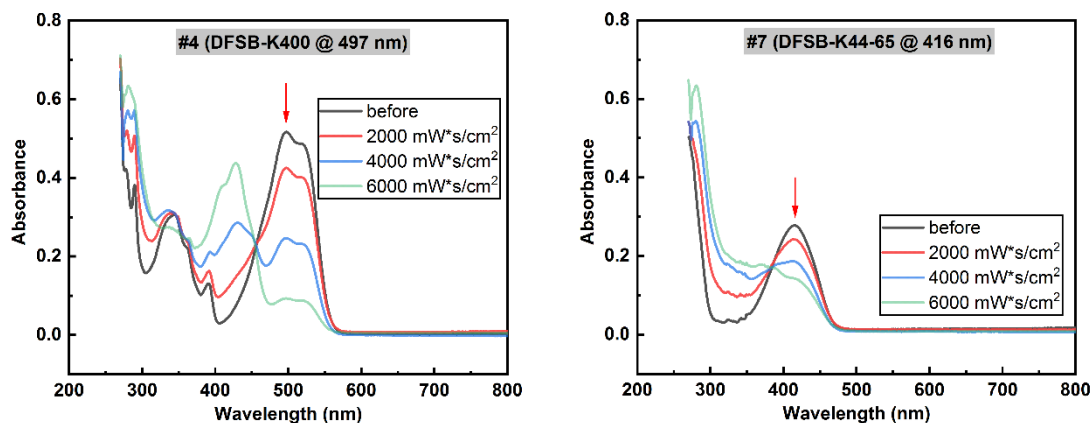
Figure ~~11~~==12==: Dye solution degradation upon UVC irradiation ~~using a UVC LED (275 nm)~~ ==with various UV radiation doses (mW·s·cm⁻²), using experimental setup displayed in figure 2.==

solution was added to a quartz cuvette. We initially used UV LEDs to irradiate the dye solution and confirm whether the selected dyes exhibited degradation upon exposure. This information guided us in designing the aerosol UV irradiation chamber. Figure ~~11~~12 presents examples of the measured UV-Vis spectra of dye solutions before and after irradiation with various UV radiation doses, using experimental setup displayed in figure 2. The higher irradiation dose required could potentially depend on the species and is also influenced by factors such as the irradiated sample volume and UV absorbance of the carrier liquid DEHS. As the UV radiation dose increased, the maximal absorbance values in the visible region decreased noticeably. Moreover, despite a similar degradation trend observed for the two tested dye solutions, at the same UV irradiation dose of 6000 mW·s·cm^{-2}, the degradation fraction for dye 4 was 90% while dye 7 was 50%. It can be concluded that dye solution #4 demonstrated a higher sensitivity to UVC irradiation at 275 nm. It is worth noting a prior study that used the degradation of water-based dye solutions to measure UV dose (Putt et al., 2012). This study irradiated a dye solution on (1 ml and 10 µg·mL^{-1}) in a quartz cuvette with 254 nm UV light. It was observed that the required UV dosage for the degradation of dye #4 (497 nm) and dye #7 (419 nm) aligns with the order of magnitude specified for Fast Green (624 nm), Allura Red (495 nm), and Tartrazine (426 nm) by the study conducted by Putt (Putt et al., 2012). While pure DEHS demonstrates significant absorbance under UVC irradiation, as shown in Figure 6a, dyes dissolved in DEHS undergo photodegradation upon UVC exposure, similar to that observed in water-dissolved dyes (Putt, et al. 2012). This behavior of dyes in DEHS under UVC irradiation might closely mimic the response of pathogens in saliva, where proteins also absorb UVC light.

Based on prior research indicating that dye #4 displayed heightened sensitivity to UVC radiation, this dye solution was chosen for aerosol droplet generation. Figure 10 displays the aerosol particle distribution produced using dye solution #4 (10 µg·mL^{-1}). The UV dose received by the droplets was estimated by multiplying the UV intensity by the average residence time of aerosols inside the exposure chamber, as summarized in Table 2. In the current study, the UV radiation dose was modulated by controlling the carrier gas flow rate, where the applied current of the UVC LED array was maintained to 1000 mA. Figure 3 illustrates both the experimental setup used and the calculated effective irradiated volume. The estimated UV radiation doses, detailed in Table 2, were 245.1 mW·s·cm^{-2} at 0.78 l·min^{-1}, 84.6 mW·s·cm^{-2} at 2.26 l·min^{-1}, and 21.6 mW·s·cm^{-2} at 8.86 l·min^{-1}, respectively. The influence of UV dose on the degradation of dye-laden aerosols can be demonstrated in Fig. ~~12~~13. Figure 13b shows an example of the UV-Vis spectra for the collected droplets, which we used to calculate the fraction of dye degradation. This calculation involved converting the maximum absorbance values at 497 nm (for dye #4) after UV irradiation (using apparatus in figure 3) into a percentage of the original absorbance value before irradiation. As depicted in figure 13a, when exposed to a 270 nm UVC array at a dose of 245.1 mW·s·cm^{-2}, an approximate 10% degradation of the dyes within the aerosols sampled was noted. Meanwhile, a lower UV dose of 21.6 mW·s·cm^{-2} was capable of degrading 5% of the dye-containing aerosol droplets. These results suggest a non-linear relationship between the ~~survival~~ degradation of UV-sensitive dyes and the increase in UV radiation doses. Two potential mathematical models that might offer insights into dye degradation: the classical exponential decay model (log-linear decay) and the shoulder model, which begins with a horizontal slope before transitioning into full exponential decay (Kowalski, 2009). However, the determination of which model is better suited for the selected dye solution remains inconclusive due to limited experimental data. A dataset that includes 90% dye degradation induced by UV radiation is, at a minimum, required. Another possible cause for the observed nonlinear degradation might be the different degradation responses in droplets of varying diameters, resulting from the

variable gas flow to the impactor, which in turn leads to different cutoff sizes for the collected droplets. Future research should also focus on optimizing the impactor to separately collect particles from different categories in order to explore potential particle size effects.

450   In addition, Figure 13b presents the UV-Vis spectra of collected aerosol droplets of both pure DEHS and dye solution #4 (10 µg·mL^{-1}) before and after UV exposure. The degradation of dye #4 after UV exposure is evidenced by noticeable changes in the maximum peak absorbance (specially at 497 nm for dye #4). While pure DEHS exhibits some spectral changes under UV irradiation, these changes are predominantly below 300 nm wavelength, with insignificant absorption changes above 400 nm. Therefore, the error introduced by using DEHS as the spectral

455   baseline for determining dye degradation is considered negligible. Besides, it's worth noting that increasing the UV dose by extending droplet residence time in the exposure section is not ideal. Observations revealed that a longer residence time (59.8 s at a gas flow of 0.78 l·min^{-1}) resulted in slightly droplets deposition on the quartz tube wall. This occurrence reduces the collection efficiency by the low-pressure impactor and diminishes the UV radiation intensity entering the chamber. Therefore, it is recommended to adjust the UV dose by altering the power

460   of UVC LEDs and limiting the residence time sedimentation loss of aerosol droplets by using a vertical UV chamber in further study.
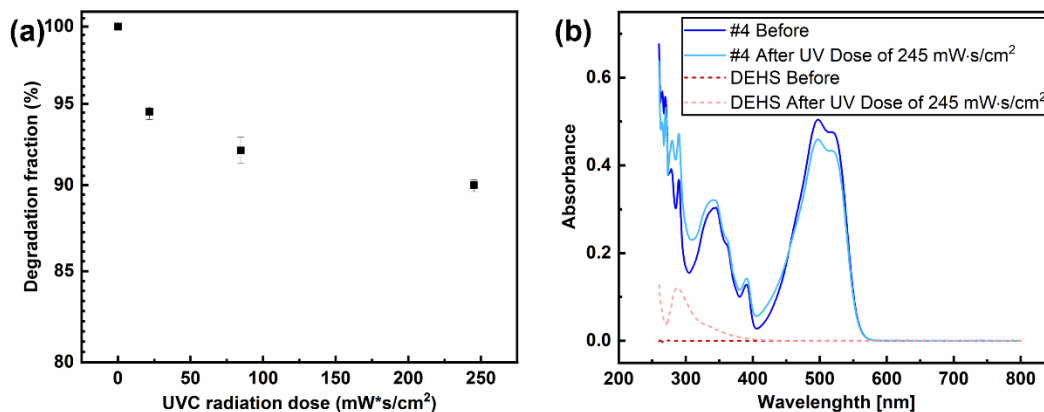
Figure 1213: (a) Effect of UVC radiation dose on the dye survival degradation within aerosol droplets and (b) UV-Vis spectra of collected aerosol droplets of both pure DEHS and dye solution #4 (10 µg·mL^{-1}) before and after UV exposure.

4 Conclusions

It is known that aerosolized viruses can effectively be disinfected by the use of UVC radiation, where its effectiveness depends on the UV dose experienced by the aerosol (Chiappa et al., 2021). The dose required for disinfection can be determined on immobilized viruses in biosafety laboratories, whereas determining the dose experienced by an aerosol in a given UV disinfection apparatus or a room equipped with UV disinfection can conveniently be done with the help of suitable nonbiogenic aerosols. Here, this study proposes a model system consisting of nonevaporating DEHS droplets containing a UV-sensitive dye. From an initial selection of 20 UV-sensitive dyes, only two were deemed suitable based on key selection criteria: prominent absorption characteristics around 260 nm and high solubility in DEHS. Moreover, it has been demonstrated that adding UV-sensitive dyes ($10\ \mu g \cdot mL^{-1}$) did not affect the particle size and number concentration of DEHS-based aerosols. For analyzing the concentration changes before and after passing through a UV irradiation chamber (with an effective UVC irradiated volume of $777\ cm^3$), a low-pressure impactor was designed to collect dye-containing aerosol droplets and transfer the liquid into a quartz cuvette. The potential of using UVC LED irradiation to degrade the UV-sensitive dye solution was also examined, leading to the development of a UV radiation chamber capable of modulating the UV dose. The self-built UVC irradiation chamber allows for the quantitative determination of the UV dose experienced by aerosols with UV-sensitive dyes. The obtained results indicate a non-linear correlation between the ~~survival~~ degradation rate of UV-sensitive dyes and the increase in UV radiation doses. Specifically, a UVC dose of $245.1\ mW \cdot s \cdot cm^{-2}$ (with an aerosol flow of $0.78\ L \cdot min^{-1}$) at 270 nm degraded approximately 10% of the dyes in DEHS aerosols, while a lower dose of $21.6\ mW \cdot s \cdot cm^{-2}$ (with an aerosol flow of $8.86\ L \cdot min^{-1}$) degraded 5% of the dye-laden aerosols. In summary, our study demonstrated the ~~feasibility of~~ approach for quantitatively determining the UV radiation dose experienced by an aerosol droplet by incorporating UV-sensitive dyes into droplets. Further research is necessary to understand the impact of the suspending medium and the aerosol droplet size on the required UV dose for dye degradation.

CRediT authorship contribution statement

Frank Einar Kruis: Supervision, Funding acquisition, Conceptualization, Review & Editing. **Qingqing Fu:** Conceptualization, Investigation, Visualization, Writing – Original draft preparation. All authors have read and agreed to the published version of the manuscript.

Declaration of competing interest

The authors declare that they have no known competing financial interests or personal relationships that could have appeared to influence the work reported in this paper.

Acknowledgement

We would like to thank "Deutsche Forschungsgemeinschaft" (DFG) for financially supporting this research project (grant no. 469047872).

References

Abkar, L., Zimmermann, K., Dixit, F., Kheyrandish, A., and Mohseni, M.: COVID-19 pandemic lesson learned-critical parameters and research needs for UVC inactivation of viral aerosols, Journal of Hazardous Materials Advances, 8, 100183, https://doi.org/10.1016/j.hazadv.2022.100183, 2022.

Ahmad, S., Ali, B., Khan, S., Fatima, A., Saeed, M., Asghar, A., Akber, S. S., Baqai, R., and Kazmi, S. U.: A Survey on Biosafety Practices in Lab Personnel in 12 Selected Areas of Karachi, Pakistan, Journal of Biosafety and Biosecurity, 1, 68–72, https://doi.org/10.1016/j.jobb.2018.12.001, 2019.

Beck, S. E., Rodriguez, R. A., Hawkins, M. A., Hargy, T. M., Larason, T. C., and Linden, K. G.: Comparison of UV-Induced Inactivation and RNA Damage in MS2 Phage across the Germicidal UV Spectrum, Appl Environ Microbiol, 82, 1468–1474, https://doi.org/10.1128/AEM.02773-15, 2016.

Biasin, M., Bianco, A., Pareschi, G., Cavalleri, A., Cavatorta, C., Fenizia, C., Galli, P., Lessio, L., Lualdi, M., Tombetti, E., Ambrosi, A., Redaelli, E. M. A., Saulle, I., Trabattoni, D., Zanutta, A., and Clerici, M.: UV-C irradiation is highly effective in inactivating SARS-CoV-2 replication, Sci Rep, 11, 6260, https://doi.org/10.1038/s41598-021-85425-w, 2021.

Bohrerova, Z., Bohrer, G., Mohanraj, S. M., Ducoste, J., and Linden, K. G.: Experimental Measurements of Fluence Distribution in a UV Reactor Using Fluorescent Microspheres, Environ. Sci. Technol., 39, 8925–8930, https://doi.org/10.1021/es050034c, 2005.

Budowsky, E. I., Bresler, S. E., Friedman, E. A., and Zheleznova, N. V.: Principles of selective inactivation of viral genome: I. UV-induced inactivation of influenza virus, Archives of Virology, 68, 239–247, https://doi.org/10.1007/BF01314577, 1981.

Buonanno, M., Welch, D., Shuryak, I., and Brenner, D. J.: Far-UVC light (222 nm) efficiently and safely inactivates airborne human coronaviruses, Sci Rep, 10, 10285, https://doi.org/10.1038/s41598-020-67211-2, 2020.

Burnett, L. C., Lunn, G., and Coico, R.: Biosafety: Guidelines for Working with Pathogenic and Infectious Microorganisms, CP Microbiology, 13, https://doi.org/10.1002/9780471729259.mc01a01s13, 2009.

Chen, B., Jia, P., and Han, J.: Role of indoor aerosols for COVID-19 viral transmission: a review, Environ Chem Lett, 19, 1953–1970, https://doi.org/10.1007/s10311-020-01174-8, 2021.

Chiappa, F., Frascella, B., Vigezzi, G. P., Moro, M., Diamanti, L., Gentile, L., Lago, P., Clementi, N., Signorelli, C., Mancini, N., and Odone, A.: The efficacy of ultraviolet light-emitting technology against coronaviruses: a systematic review, Journal of Hospital Infection, 114, 63–78, https://doi.org/10.1016/j.jhin.2021.05.005, 2021.

Darnell, M. E. R. and Taylor, D. R.: Evaluation of inactivation methods for severe acute respiratory syndrome coronavirus in noncellular blood products, Transfusion, 46, 1770–1777, https://doi.org/10.1111/j.1537-2995.2006.00976.x, 2006.

Deshmukh, D. R. and Pomeroy, B. S.: Ultraviolet Inactivation and Photoreactivation of Avian Viruses, Avian Diseases, 13, 596, https://doi.org/10.2307/1588533, 1969.

Dong, E., Du, H., and Gardner, L.: An interactive web-based dashboard to track COVID-19 in real time, The Lancet Infectious Diseases, 20, 533–534, https://doi.org/10.1016/S1473-3099(20)30120-1, 2020.

Eickmann, M., Gravemann, U., Handke, W., Tolksdorf, F., Reichenberg, S., Müller, T. H., and Seltsam, A.: Inactivation of three emerging viruses – severe acute respiratory syndrome coronavirus, Crimean–Congo haemorrhagic fever virus and Nipah virus – in platelet concentrates by ultraviolet C light and in plasma by methylene blue plus visible light, Vox Sang, 115, 146–151, https://doi.org/10.1111/vox.12888, 2020.

Fabian, P., Brain, J., Houseman, E. A., Gern, J., and Milton, D. K.: Origin of Exhaled Breath Particles from Healthy and Human Rhinovirus-Infected Subjects, Journal of Aerosol Medicine and Pulmonary Drug Delivery, 24, 137–147, https://doi.org/10.1089/jamp.2010.0815, 2011a.

Fabian, P., Brain, J., Houseman, E. A., Gern, J., and Milton, D. K.: Origin of Exhaled Breath Particles from Healthy and Human Rhinovirus-Infected Subjects, Journal of Aerosol Medicine and Pulmonary Drug Delivery, 24, 137–147, https://doi.org/10.1089/jamp.2010.0815, 2011b.

Feng, Y., Smith, D. W., and Bolton, J. R.: A Potential New Method for Determination of the Fluence (UV Dose) Delivered in UV Reactors Involving the Photodegradation of Free Chlorine, Water Environment Research, 82, 328–334, https://doi.org/10.2175/106143009X447920, 2010.

Ferron, G. A. and Soderholm, S. C.: Estimation of the times for evaporation of pure water droplets and for stabilization of salt solution particles, Journal of Aerosol Science, 21, 415–429, https://doi.org/10.1016/0021-8502(90)90070-E, 1990.

Fujimoto, N., Nagaoka, K., Tatsuno, I., Oishi, H., Tomita, M., Hasegawa, T., Tanaka, Y., and Matsumoto, T.: Wavelength dependence of ultraviolet light inactivation for SARS-CoV-2 omicron variants, Sci Rep, 13, 9706, https://doi.org/10.1038/s41598-023-36610-6, 2023.

Gandhi, V. N., Roberts, P. J. W., and Kim, J.-H.: Visualizing and Quantifying Dose Distribution in a UV Reactor Using Three-Dimensional Laser-Induced Fluorescence, Environ. Sci. Technol., 46, 13220–13226, https://doi.org/10.1021/es303133f, 2012.

Gustavsson, J.: EN 779:2002 — New European test method for air filters, Filtration & Separation, 40, 22–26, https://doi.org/10.1016/S0015-1882(03)80065-4, 2003.

Hamzavi, I. H., Lyons, A. B., Kohli, I., Narla, S., Parks-Miller, A., Gelfand, J. M., Lim, H. W., and Ozog, D. M.: Ultraviolet germicidal irradiation: Possible method for respirator disinfection to facilitate reuse during the COVID-19 pandemic, Journal of the American Academy of Dermatology, 82, 1511–1512, https://doi.org/10.1016/j.jaad.2020.03.085, 2020.

Helsper, C., Mölter, W., and Haller, P.: Representative dilution of aerosols by a factor of 10,000, Journal of Aerosol Science, 21, S637–S640, https://doi.org/10.1016/0021-8502(90)90323-P, 1990.

Hemdan, S. S.: The Shift in the Behavior of Methylene Blue Toward the Sensitivity of Medium: Solvatochromism, Solvent Parameters, Regression Analysis and Investigation of Cosolvent on the Acidity Constants, J Fluoresc, 33, 2489–2502, https://doi.org/10.1007/s10895-023-03234-y, 2023.

Heßling, M., Hönes, K., Vatter, P., and Lingenfelder, C.: Ultraviolet irradiation doses for coronavirus inactivation – review and analysis of coronavirus photoinactivation studies, GMS Hygiene and Infection Control; 15:Doc08, https://doi.org/10.3205/DGKH000343, 2020.

Hijnen, W. A. M., Beerendonk, E. F., and Medema, G. J.: Inactivation credit of UV radiation for viruses, bacteria and protozoan (oo)cysts in water: A review, Water Research, 40, 3–22, https://doi.org/10.1016/j.watres.2005.10.030, 2006.

Inagaki, H., Saito, A., Sugiyama, H., Okabayashi, T., and Fujimoto, S.: Rapid inactivation of SARS-CoV-2 with deep-UV LED irradiation, Emerging Microbes & Infections, 9, 1744–1747, https://doi.org/10.1080/22221751.2020.1796529, 2020.

Kariwa, H., Fujii, N., and Takashima, I.: Inactivation of SARS Coronavirus by Means of Povidone-Iodine, Physical Conditions and Chemical Reagents, Dermatology, 212, 119–123, https://doi.org/10.1159/000089211, 2006.

Kaur, S. P. and Gupta, V.: COVID-19 Vaccine: A comprehensive status report, Virus Research, 288, 198114, https://doi.org/10.1016/j.virusres.2020.198114, 2020.

Kim, D.-K. and Kang, D.-H.: UVC LED Irradiation Effectively Inactivates Aerosolized Viruses, Bacteria, and Fungi in a Chamber-Type Air Disinfection System, Appl Environ Microbiol, 84, e00944-18, https://doi.org/10.1128/AEM.00944-18, 2018.

Kowalski, W.: Ultraviolet Germicidal Irradiation Handbook: UVGI for Air and Surface Disinfection, Springer Berlin Heidelberg, Berlin, Heidelberg, https://doi.org/10.1007/978-3-642-01999-9, 2009.

590   Kowalski, W.: Performance of the UV24 Unit Against Zoonotic Pathogens, San Fernando, CA: Medical Illumination. 2017 Feb 1, Available from: http://www.medillum.com/wp-content/uploads/2017/03/Performance-of-the-UV24-Unit-Against-Zoonotic-Pathogens.pdf

Kurz, W., Yetisen, A. K., Kaito, M. V., Fuchter, M. J., Jakobi, M., Elsner, M., and Koch, A. W.: UV-Sensitive Wearable Devices for Colorimetric Monitoring of UV Exposure, Adv. Optical Mater., 8, 1901969, https://doi.org/10.1002/adom.201901969, 2020.

595   Kyrychenko, A.: Using fluorescence for studies of biological membranes: a review, Methods Appl. Fluoresc., 3, 042003, https://doi.org/10.1088/2050-6120/3/4/042003, 2015.

Lefebvre, X., Succar, A., Bédard, E., Prévost, M., and Robert, E.: Characterization of drying bioaerosols with four size distribution measurement instruments in the context of airborne transmission, In Review, https://doi.org/10.21203/rs.3.rs-2207576/v1, 2022.

600   Leung, W. W. F. and Sun, Q.: Electrostatic charged nanofiber filter for filtering airborne novel coronavirus (COVID-19) and nano-aerosols, Separation and Purification Technology, 250, 116886, https://doi.org/10.1016/j.seppur.2020.116886, 2020.

Li, L., Lee, E. S., Nguyen, C., and Zhu, Y.: Effects of propylene glycol, vegetable glycerin, and nicotine on emissions and dynamics of electronic cigarette aerosols, Aerosol Science and Technology, 54, 1270–1281,
605   https://doi.org/10.1080/02786826.2020.1771270, 2020.

~~Mankar, V., Dhengre, A., Agashe, N., Rodge, H., and Chandi, D. H.: Ultraviolet irradiation doses for coronavirus inactivation review and analysis of coronavirus photo inactivation studies, ijhs, 466-472, https://doi.org/10.53730/ijhs.v6nS2.5038, 2022.~~

Morawska, L., Johnson, G. R., Ristovski, Z. D., Hargreaves, M., Mengersen, K., Corbett, S., Chao, C. Y. H., Li,
610   Y., and Katoshevski, D.: Size distribution and sites of origin of droplets expelled from the human respiratory tract during expiratory activities, Journal of Aerosol Science, 40, 256–269, https://doi.org/10.1016/j.jaerosci.2008.11.002, 2009.

Muñoz, M., Comtois-Bona, M., Cortes, D., Cimenci, C. E., Du, Q., Thompson, C., Figueroa, J. D., Franklin, V., Liu, P., and Alarcon, E. I.: Integrated photothermal decontamination device for N95 respirators, Sci Rep, 11, 1822,
615   https://doi.org/10.1038/s41598-020-80908-8, 2021.

Pratelli, A.: Canine coronavirus inactivation with physical and chemical agents, The Veterinary Journal, 177, 71–79, https://doi.org/10.1016/j.tvjl.2007.03.019, 2008.

Priya, S. S., Cuce, E., and Sudhakar, K.: A perspective of COVID 19 impact on global economy, energy and environment, International Journal of Sustainable Engineering, 14, 1290–1305,
620   https://doi.org/10.1080/19397038.2021.1964634, 2021.

Putt, K. S., Kernick, E. R., Lohse, B. K., Lomboy, J., O'Brien, T., and Pugh, R. B.: The use of chromophore and fluorophore degradation to quantitate UV dose: FD&C dyes as chemical identicators for UV sterilization, Journal of Microbiological Methods, 91, 215–221, https://doi.org/10.1016/j.mimet.2012.08.015, 2012.

Reed, N. G.: The History of Ultraviolet Germicidal Irradiation for Air Disinfection, Public Health Rep, 125, 15–
625   27, https://doi.org/10.1177/003335491012500105, 2010.

Ren, J., He, J., Li, J., and Liu, J.: A Method to Generate Experimental Aerosol with Similar Particle Size Distribution to Atmospheric Aerosol, Atmosphere, 12, 1669, https://doi.org/10.3390/atmos12121669, 2021.

Song, K., Mohseni, M., and Taghipour, F.: Application of ultraviolet light-emitting diodes (UV-LEDs) for water disinfection: A review, Water Research, 94, 341–349, https://doi.org/10.1016/j.watres.2016.03.003, 2016.

630   Stegemann, S., Leveiller, F., Franchi, D., De Jong, H., and Lindén, H.: When poor solubility becomes an issue: From early stage to proof of concept, European Journal of Pharmaceutical Sciences, 31, 249–261, https://doi.org/10.1016/j.ejps.2007.05.110, 2007.

635 Talaat, K., Xi, J., Baldez, P., and Hecht, A.: Radiation Dosimetry of Inhaled Radioactive Aerosols: CFPD and MCNP Transport Simulations of Radionuclides in the Lung, Sci Rep, 9, 17450, https://doi.org/10.1038/s41598-019-54040-1, 2019.

Terpstra, F. G., Van 'T Wout, A. B., Schuitemaker, H., Van Engelenburg, F. A. C., Dekkers, D. W. C., Verhaar, R., De Korte, D., and Verhoeven, A. J.: Potential and limitation of UVC irradiation for the inactivation of pathogens in platelet concentrates, Transfusion, 0, 071121030748013-???, https://doi.org/10.1111/j.1537-2995.2007.01524.x, 2007.

640 Tseng, C.-C. and Li, C.-S.: Inactivation of Virus-Containing Aerosols by Ultraviolet Germicidal Irradiation, Aerosol Science and Technology, 39, 1136–1142, https://doi.org/10.1080/02786820500428575, 2005.

Van Dorp, L., Acman, M., Richard, D., Shaw, L. P., Ford, C. E., Ormond, L., Owen, C. J., Pang, J., Tan, C. C. S., Boshier, F. A. T., Ortiz, A. T., and Balloux, F.: Emergence of genomic diversity and recurrent mutations in SARS-CoV-2, Infection, Genetics and Evolution, 83, 104351, https://doi.org/10.1016/j.meegid.2020.104351, 2020.

645 Verreault, D., Moineau, S., and Duchaine, C.: Methods for Sampling of Airborne Viruses, Microbiol Mol Biol Rev, 72, 413–444, https://doi.org/10.1128/MMBR.00002-08, 2008.

Walker, C. M. and Ko, G.: Effect of Ultraviolet Germicidal Irradiation on Viral Aerosols, Environ. Sci. Technol., 41, 5460–5465, https://doi.org/10.1021/es070056u, 2007.

Wang, C. C., Prather, K. A., Sznitman, J., Jimenez, J. L., Lakdawala, S. S., Tufekci, Z., and Marr, L. C.: Airborne 650 transmission of respiratory viruses, Science, 373, eabd9149, https://doi.org/10.1126/science.abd9149, 2021.

Wang, J., Jeevarathinam, A. S., Jhunjhunwala, A., Ren, H., Lemaster, J., Luo, Y., Fenning, D. P., Fullerton, E. E., and Jokerst, J. V.: A Wearable Colorimetric Dosimeter to Monitor Sunlight Exposure, Adv. Mater. Technol., 3, 1800037, https://doi.org/10.1002/admt.201800037, 2018.

Welch, D., Buonanno, M., Grilj, V., Shuryak, I., Crickmore, C., Bigelow, A. W., Randers-Pehrson, G., Johnson, 655 G. W., and Brenner, D. J.: Far-UVC light: A new tool to control the spread of airborne-mediated microbial diseases, Sci Rep, 8, 2752, https://doi.org/10.1038/s41598-018-21058-w, 2018.

Zayas, G., Chiang, M. C., Wong, E., MacDonald, F., Lange, C. F., Senthilselvan, A., and King, M.: Cough aerosol in healthy participants: fundamental knowledge to optimize droplet-spread infectious respiratory disease management, BMC Pulm Med, 12, 11, https://doi.org/10.1186/1471-2466-12-11, 2012.

660 Zheng, D., Yuan, X.-A., Ma, H., Li, X., Wang, X., Liu, Z., and Ma, J.: Unexpected solvent effects on the UV/Vis absorption spectra of o-cresol in toluene and benzene: in contrast with non-aromatic solvents, R. Soc. open sci., 5, 171928, https://doi.org/10.1098/rsos.171928, 2018.